Wireless Pers Commun (2013) 71:1487–1503
DOI 10.1007/s11277-012-0887-9

Distance Distribution in Convex n-Gons: Mathematical Framework and Wireless Networking Applications

Konstantinos B. Baltzis

Published online: 19 October 2012

Abstract The performance of a wireless network is related to the Euclidean distance distribution between the communication nodes, which in turn depends on network geometry. In this paper, we provide an analytical framework for the description of distance statistics in convex polygons with arbitrary number and length of sides. Simulation results validate the formulation. Comparisons with models in the literature indicate that our approach is a generalization of previous works. Representative examples show the merits of the proposal and assess its applicability in wireless networking. The main contribution of this work is the consideration of polygonal-shaped networks. The obtained formulation reduces the complexity and computational cost of the modeling and simulation of wireless systems and it is more convenient than other approaches when network planning considers n-gonal coverage areas. Moreover, it provides adequate results for the calculation of distance-dependent parameters and performance metrics of wireless networks.

Keywords Euclidean distance · Polygon · Distance-related metrics · Routing protocol · Voronoi diagram · Wireless network

1 Introduction

The advances in wireless networks have resulted in a significant increase in the required recourses and effort for their design and study. These demands are usually met through the use of powerful computer-aided analysis tools, but at the same time, several research attempts target to the analytical description of system characteristics and performance metrics so as to reduce the required complexity and computational cost for their analysis and study.

A topic that has been extensively studied in the past is the internode distance distribution. This knowledge is crucial in system configuration, protocol design, resource management

K. B. Baltzis (✉)
Radio Communications Laboratory, Department of Physics, Aristotle University of Thessaloniki, Thessaloniki, Greece
e-mail: kmpal@physics.auth.gr

and throughput analysis. In fact, distance statistics are related to several topics in wireless networking such as coverage [1,2], connectivity [2–4], capacity [3,5], spectral efficiency [3,6], power consumption [4,7–9], interference [3–6,10], error probability [10,11], path loss estimation [6,10,12,13], routing [3,4,7–9,11,14,15] and localization [4,9,14].

Distance distribution depends on network shape. In practice, the coverage area of a wireless network is irregularly shaped and influenced by man-made structures and terrain contour. However, approximate methods are often suggested for analytical convenience. A simplistic approach is the circular one [6,10,12,16] and it rises from the fact that the coverage area of an omni-directional transmitter is, ideally, a circular disk. The hexagonal approximation [5,13,15–17] is flexible and convenient and allows the coverage of the network area without gaps. This is employed in the planning and analysis of cellular networks such as in macrocellular ones with base station antennas placed at great height. Another reasonable assumption, esp. for small-scale networks in indoor environments, is the rectangular-shaped networks [8,15,18,19]. The approach provides full network coverage and it is simpler than the previous one. In hexagonal tessellations, the covered area may also be described by rhombuses when directional antennas are employed [15,20,21]. Rhombuses are further used in the study of wireless sensor networks (WSNs) for the sake of deployment convenience and increased connectivity [2,20]. However, the coverage area of WSNs usually comprises Voronoi polygons [11,22–24] to assure full network coverage and reduced energy consumption. In highly non-static systems, such as mobile and vehicular ad hoc networks, and in WSNs with mobile nodes that are relocated from their initial deployment locations for coverage improvement, the nodes are distributed according to a stochastic process (Poisson, Gaussian, etc.) [3,4,25,26].

In this paper, we consider that the communication nodes are distributed within an area bounded by an arbitrary convex polygon of n sides (n-gon). The purpose of this paper is twofold. First, we provide analytical expressions for the Euclidean distance density (pdf) and distribution (cdf) from a fixed point within a region bounded from an n-gon. Comparisons with simulation results and models in the literature validate the model. Then, the obtained formulation is used to describe certain distance-dependent network parameters and performance metrics assuming uniform node distribution,[1] and their application in radio propagation, WSNs' sensitivity, network routing and energy consumption.

The proposed model suits for the design, analysis and simulation of polygonal-shaped networks. Applications can be found in areas such as WSNs, mobile ad hoc networking and irregular (non-uniform) cellular systems. The obtained results can also be viewed as a generalization of recent works in computational geometry and their application in the study of wireless networks with simpler geometric layouts such as hexagonal, square and circular ones. The analytical description of distance statistics and performance metrics simplifies the analysis and simulation of a wireless network and reduces the computational requirements. The calculated results are exact, they do not require further statistical inspection and they can be used as first-order approximation for more complex models and real nodes distributions [28]. Moreover, the derived formulation is more convenient than other approaches when network planning assumes n-gonal coverage areas (Voronoi polygons, for example).

The rest of the paper is organized as follows: Sect. 2 presents related work in the area. Section 3 derives the probabilistic distance distributions for the proposed model. In Sect. 4, we provide comparisons with simulation results and models in the literature. Section 5 discusses representative applications in wireless networking. Finally, Sect. 6 concludes the paper.

[1] This assumption is quite common in the literature; see, for example, [2,4–13,15–19,21,24,25,27].

2 Related Work

The knowledge of the internode distance distribution is essential for the design, analysis and performance evaluation of a wireless network. The network geometry plays an important role in the determination of the distance statistics. Thus, despite the fact that there are infinite network shapes, the assumption of regular-shaped ones that allows an analytical description of networks characteristics and performance metrics is popular because it reduces the computational requirements, provides key insights into the stochastic characteristics of the system and, in general, gives adequate results.

This issue is concisely treated in the published literature. Next, we give the pdf of the distance from a fixed reference point within a region bounded from a circle, a square and a hexagon. In a circular disk of radius R, the pdf of the distance d from a fixed point located at a distance $D \leq R$ from the center of the circle is [10]

$$f_c(d) = \begin{cases} \frac{2d}{R^2}, & d \leq R - D \\ \frac{2d}{\pi R^2} \cos^{-1}\left(\frac{d^2+D^2-R^2}{2Dd}\right), & R - D < d \leq R + D \end{cases} \tag{1}$$

In a square with side a, the Euclidean distance densities from the center of the square, a midpoint of a side, and a square vertex, are, respectively, [19]:

$$f_{s,c}(d) = \begin{cases} \frac{2\pi d}{a^2}, & d \leq \frac{a}{2} \\ \frac{2\pi d}{a^2}\left[1 - \frac{4}{\pi}\cos^{-1}\left(\frac{a}{2d}\right)\right], & \frac{a}{2} < d \leq \frac{a}{\sqrt{2}} \end{cases} \tag{2}$$

$$f_{s,m}(d) = \begin{cases} \frac{\pi d}{a^2}, & d \leq \frac{a}{2} \\ \frac{\pi d}{a^2}\left[1 - \frac{2}{\pi}\cos^{-1}\left(\frac{a}{2d}\right)\right], & \frac{a}{2} < d \leq a \\ \frac{\pi d}{a^2}\left[1 - \frac{4}{\pi}\cos^{-1}\left(\frac{a}{2d}\right)\right], & a < d \leq \frac{\sqrt{5}a}{2} \end{cases} \tag{3}$$

$$f_{s,v}(d) = \begin{cases} \frac{\pi d}{2a^2}, & d \leq a \\ \frac{\pi d}{2a^2}\left[1 - \frac{4}{\pi}\cos^{-1}\left(\frac{a}{d}\right)\right], & a < d \leq \sqrt{2}a \end{cases} \tag{4}$$

Finally, the pdf of the distance from a vertex or the center of a hexagon are [5,13]

$$f_{h,v}(d) = \begin{cases} \frac{\pi d}{3\sqrt{3}\rho^2}, & d \leq \frac{2\rho}{\sqrt{3}} \\ \frac{d}{\sqrt{3}\rho^2}\sin^{-1}\left(\frac{\rho}{d}\right), & \frac{2\rho}{\sqrt{3}} < d \leq 2\rho \\ \frac{d}{\sqrt{3}\rho^2}\left[\frac{\pi}{6} - \sin^{-1}\left(\sqrt{1 - \left(\frac{2\rho}{d}\right)^2}\right)\right], & 2\rho < d \leq \frac{4\rho}{\sqrt{3}} \end{cases} \tag{5}$$

and

$$f_{h,c}(d) = \begin{cases} \frac{\pi d}{\sqrt{3}\rho^2}, & d \leq \rho \\ \frac{2\sqrt{3}d}{\rho^2}\left[\frac{\pi}{6} - \cos^{-1}\left(\frac{\rho}{d}\right)\right], & \rho < d \leq \frac{2\rho}{\sqrt{3}} \end{cases} \tag{6}$$

respectively, where ρ is the inradius of the hexagon. Under the assumption of uniform node distribution, (1)–(6) describe the internode distance pdf in wireless networks with the aforementioned geometries.

The previous formulas are used for the description of distance statistics in networks with simple geometric layouts. However, none of these expressions can be generalized to complex systems due to the constraints imposed by the systems' geometry. A more general model for the description of distance distribution in complex systems follows.

3 The Proposed Model

In this section, we provide analytical expressions for the cdf and pdf of the distance between a fixed reference point and a random point within a convex n-gonal region, such as a Voronoi polygon; see Fig. 1. The formulation is also applicable in regular-shaped networks such as hexagonal, rectangular, etc. (see, next section).

We consider a polar coordinates system with its origin at a fixed reference point O bounded from an n-gon with vertices at (r_i, φ_i), $i = 1 \ldots n$. The cdf $F_p(d)$ of the distance d between O and a random point within the n-gonal region is given by the ratio of the overlapping area between a circle with radius d centered at O (let us call this circle $\mathbf{C}(\mathrm{O}, d)$) and the n-gon, to the area of the n-gon. The first is the sum of the overlapping areas A_i, $i = 1 \ldots n$, between the circle and each of the n triangles with vertices at $(0, 0)$, (r_i, φ_i) and (r_{i+1}, φ_{i+1}) (it is $r_{n+1} = r_1$ and $\varphi_{n+1} = \varphi_1$). Thus, $F_p(d)$ is

$$F_p(d) = 2\left(\sum_{i=1}^{n} r_i r_{i+1} \sin \varphi_{i+1,i}\right)^{-1} \sum_{i=1}^{n} A_i \tag{7}$$

where $\varphi_{i,j} = \varphi_i - \varphi_j$ and $\sum_{i=1}^{n} r_i r_{i+1} \sin \varphi_{i+1,i}/2$ is the area of the n-gon.

In order to calculate $F_p(d)$, we first find the area A_t of the overlapping region of a triangle with vertices at $\mathrm{O}(0, 0)$, $\mathrm{A}(r_1, \varphi_1)$ and $\mathrm{B}(r_2, \varphi_2)$ and the circle $\mathbf{C}(\mathrm{O}, d)$, see Fig. 2. We assume that $r_1 \leq r_2$ and $0 \leq \varphi_1 < \varphi_2 \leq \pi/2$. We distinguish four different cases depending on the overlap between the two shapes: the circle intersects with the triangle only at the sides OA and OB at $\mathrm{C}(d_1, \varphi_1)$ and $\mathrm{D}(d_1, \varphi_2)$, respectively, the circle intersects the triangle at the side AB at two points, the $\mathrm{F}(d_2, \varphi_{d1})$ and $\mathrm{G}(d_2, \varphi_{d2})$, or at one point, the $\mathrm{J}(d_3, \varphi_{d3})$, and, finally, the triangle is inside the circle.

In the first case ($d = d_1$ in Fig. 2), the circle $\mathbf{C}(\mathrm{O}, d)$ does not intersect with AB. The intersection region is the circular sector OCD with area

$$A_t = \frac{1}{2}\varphi_{2,1} d^2 \tag{8}$$

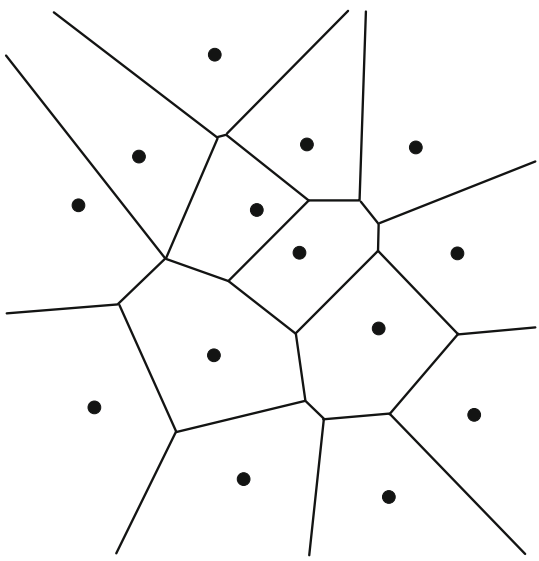

Fig. 1 Voronoi diagram for a set of 14 arbitrary positioned nodes [29]

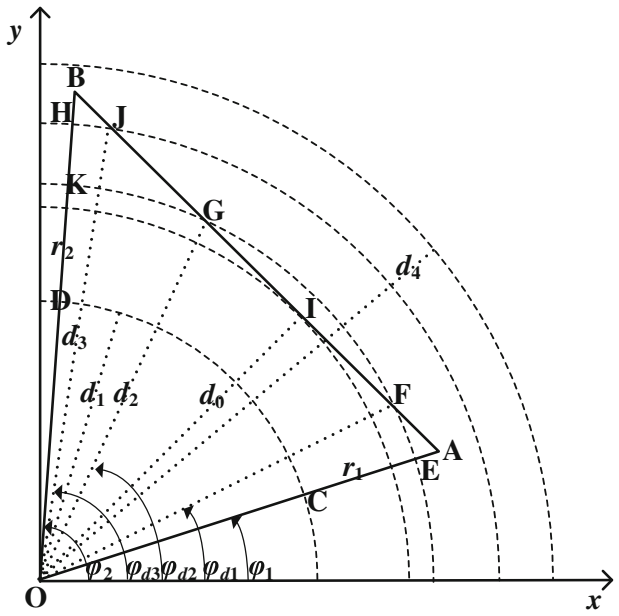

Fig. 2 Circle-triangle intersection cases

where d ranges from 0 to an upper limit which is the radial coordinate d_0 of the tangent point when AB is tangent to $\mathbf{C}\,(\mathrm{O}, d_0)$ (point I in Fig. 2); otherwise, it is the r_1. The first occurs when the opposite angle to OB is acute which happens if the side OA is larger than the projection of OB on OA, i.e., for $r_1 > r_2 \cos\phi_{21}$. The distance d_0 is calculated [30] from the expression

$$[d_0 d\ (\mathrm{A}, \mathrm{B})]^2 - [\det\ (\mathrm{A}, \mathrm{B})]^2 = 0 \tag{9}$$

with d (A, B) the Euclidean distance between points A (r_1, φ_1) and B (r_2, φ_2) and det (A,B) the determinant of the 2×2 matrix with elements the polar coordinates of the two points. After some algebraic manipulation, (9) gives that

$$d_0 = \frac{r_1 r_2 \sin\varphi_{2,1}}{\sqrt{r_1^2 + r_2^2 - 2r_1 r_2 \cos\varphi_{2,1}}} \tag{10}$$

The circle $\mathbf{C}\,(\mathrm{O}, d)$ intersects the side AB at two points only when the interior angle between OA and AB is acute (this happens for $d \in (d_0, r_1]$ when $r_1 > r_2 \cos\phi_{21}$). In this case ($d = d_2$ in Fig. 2), the overlapping region is the triangle OFG and the circular sectors OEF and OGK. Its area is given by

$$A_t = \frac{1}{2}\left(\sin\varphi_{d2,d1} + \varphi_{2,1} - \varphi_{d2,d1}\right) d^2 \tag{11}$$

where φ_{d1} and φ_{d2} ($\varphi_{d2} > \varphi_{d1}$) are the azimuths of points F and G, respectively. In order to calculate them, we should express AB in polar coordinates. The two-point form of a straight line $r = r\,(\varphi)$ through the points with polar coordinates (r_1, φ_1) and (r_2, φ_2) is

$$r\sin\varphi - r_1\sin\varphi_1 = \frac{r_2\sin\varphi_2 - r_1\sin\varphi_1}{r_2\cos\varphi_2 - r_1\cos\varphi_1}\left(r\cos\varphi - r_1\cos\varphi_1\right) \tag{12}$$

that gives

$$r_{\mathrm{AB}} = \frac{c_1}{\sin\varphi - c_2\cos\varphi} \tag{13}$$

with $c_1 = \frac{r_1 r_2 \sin\varphi_{2,1}}{r_1\cos\varphi_1 - r_2\cos\varphi_2}$ and $c_2 = \frac{r_1\sin\varphi_1 - r_2\sin\varphi_2}{r_1\cos\varphi_1 - r_2\cos\varphi_2}$. It can easily be shown, that (13) can be written in quadratic from as

$$\sin^2\varphi - \frac{2c_1}{\left(1+c_2^2\right)r_{\mathrm{AB}}}\sin\varphi + \frac{c_1^2 - c_2^2 r_{\mathrm{AB}}^2}{\left(1+c_2^2\right)r_{\mathrm{AB}}^2} = 0 \tag{14}$$

The roots of (14) for $r_{\mathrm{AB}} = d$, φ_{d1} and φ_{d2}, are

$$\varphi_d^{\pm} = \sin^{-1}\left(\frac{c_1 \pm c_2\sqrt{\left(1+c_2^2\right)d^2 - c_1^2}}{\left(1+c_2^2\right)d}\right), \quad \varphi_d^{\pm} \in \left[0, \frac{\pi}{2}\right] \tag{15}$$

with $\varphi_{d1} = \varphi_d^-$ and $\varphi_{d2} = \varphi_d^+$ when c_2, i.e., the slope of AB, is positive and vice versa for negative c_2.

The circle $\mathbf{C}\,(\mathrm{O}, d)$ intersects the triangle OAB at a single point at AB when $d \in (r_1, r_2)$ under the constraint $r_1 \neq r_2$. In this case ($d = d_3$ in Fig. 2), the intersection region is the triangle OAJ and the circular sector OJH. The area of this region is

$$A_t = \frac{1}{2}d\left(\varphi_{2,d3}d + r_1\sin\varphi_{d3,1}\right) \tag{16}$$

where φ_{d3} is the root of (14) within the range (φ_1, φ_2).

Finally, for $d > r_2$ ($d = d_4$ in Fig. 2) the circle covers the whole triangle that gives

$$A_t = \frac{1}{2}r_1 r_2\sin\varphi_{2,1} \tag{17}$$

In the previous analysis, we assumed that $\varphi_{2,1} \leq \pi/2$. In order to generalize for $\varphi_{2,1} > \pi/2$, we consider that the axis $\varphi = \pi/2$ splits the triangle OAB into two new ones and then we calculate the overlapping area from the intersection of the circle $\mathbf{C}(\mathrm{O}, d)$ with each of the triangles. By setting $\varphi = \pi/2$ in (13), we get that the length of the common side of the triangles is c_1. Thus, their vertices coordinates are $(0, 0)$, (c_1, φ_1), $(c_1, \pi/2)$ and $(0, 0)$, $(r_2, \pi - \varphi_2)$, $(c_1, \pi/2)$.

The formulation for $r_1 > r_2$ is similarly obtained. In the general case, it can easily be shown that the area of the intersection region between the circle $\mathbf{C}\,(\mathrm{O}, d)$ and the triangle OAB is a piecewise function defined as

$$A_t = \begin{cases} \frac{1}{2}\left[\varphi_{2,1} + F\left(\varphi_{d1}, \varphi_{d2}\right)\right]d^2, & d \leq r_d \\ \frac{1}{2}\mathrm{sgn}\left(\varphi_{d3,0}\right)\left(\varphi_{d3,0}d - r_d\sin\bar{\varphi}_{d3,0}\right)d, & r_d < d < r_u \\ \frac{1}{2}r_1 r_2\sin\varphi_{2,1}, & d \geq r_u \end{cases} \tag{18}$$

where $\varphi_{d3,0}$ and $\bar{\varphi}_{d3,0}$ are $\varphi_{d3} - \varphi_2$ and $\varphi_{d3} - \varphi_1$, respectively, if $r_1 < r_2$ and vice versa when $r_1 \geq r_2$, $\mathrm{sgn}\,(\cdot)$ is the signum function, $r_d = \min\,(r_1, r_2)$, $r_u = \max\,(r_1, r_2)$ and

$$F\left(\varphi_{d1}, \varphi_{d2}\right) = \begin{cases} \sin\varphi_{d2,d1} - \varphi_{d2,d1}, & d > d_0 \text{ and } r_d > r_u\cos\varphi_{21} \\ 0, & \text{otherwise} \end{cases} \tag{19}$$

As a result of the rotational symmetry of the model, the area A_t does not depend on the values of φ_1 and φ_2 but on their difference $\varphi_{2,1}$. Therefore, each A_i term in (7) may be obtained by setting $r_1 = r_i$, $r_2 = r_{i+1}$, $\varphi_1 = 0$ and $\varphi_2 = \varphi_{i+1,i}$, $i = 1 \ldots n$, in (18).

The distance pdf $f_p(d)$ is the partial derivative of $F_p(d)$ with respect to d, i.e.,

$$f_p(d) = 2\left(\sum_{i=1}^{n} r_i r_{i+1} \sin\varphi_{i+1,i}\right)^{-1} \sum_{i=1}^{n} \frac{\partial A_i}{\partial d} \tag{20}$$

After some manipulation, we get from (15), (18) and (19) that

$$\frac{\partial A_t}{\partial d} = \begin{cases} \left(\varphi_{2,1} + F(\varphi_{d1}, \varphi_{d2}) + \frac{d}{2}\frac{\partial F(\varphi_{d1},\varphi_{d2})}{\partial d}\right) d, & d \le r_d \\ \frac{1}{2}\mathrm{sgn}\left(\varphi_{d3,0}\right)\left(2\varphi_{d3,0}d - r_d \sin\bar{\varphi}_{d3,0} + d\left(d - r_d\cos\bar{\varphi}_{d3,0}\right)\frac{\partial\varphi_{d3}}{\partial d}\right), & r_d < d < r_u \\ 0, & d \ge r_u \end{cases} \tag{21}$$

where

$$\frac{\partial F(\varphi_{d1}, \varphi_{d2})}{\partial d} = \begin{cases} \frac{2c_1(\cos\varphi_{d2,d1}-1)}{d\sqrt{(1+c_2^2)d^2 - c_1^2}}, & d > d_0 \text{ and } r_d > r_u\cos\varphi_{21} \\ 0, & \text{otherwise} \end{cases} \tag{22}$$

and $\partial\varphi_{d3}/\partial d$ is, depending on the value of φ_{d3}, equal to $\partial\varphi_d^+/\partial d$ or $\partial\varphi_d^-/\partial d$, with

$$\frac{\partial\varphi_d^{\pm}}{\partial d} = \mathrm{sgn}\left(\pm c_1 c_2 - \sqrt{\left(1+c_2^2\right)d^2 - c_1^2}\right)\frac{c_1}{d\sqrt{\left(1+c_2^2\right)d^2 - c_1^2}} \tag{23}$$

The $\partial A_i/\partial d$ terms in (20) are obtained by setting $r_1 = r_i$, $r_2 = r_{i+1}$, $\varphi_1 = 0$ and $\varphi_2 = \varphi_{i+1,i}$, $i = 1\ldots n$, in (21). Moreover, if $\varphi_{i+1,i} > \pi/2$, we split the triangle into two new ones and calculate the $\partial A_i/\partial d$ as a sum of two terms that correspond to the intersections of the circle $\mathbf{C}(\mathrm{O}, d)$ with each of the new triangles.

The validation of (7) and (20) through comparisons with simulation results follows in the next section. In the same section, we further show that the proposed model extends previous proposals in the published literature.

4 Model Validation

In order to validate our model, we performed Monte-Carlo simulations [31] for different n-gons. Here, we show the results for two representative cases. System parameters were chosen so as to verify the accuracy of the model in a complex system. In particular, we consider a pentagon and a heptagon, scenarios #1 and #2, respectively, with vertices coordinates (r_i, φ_i), $i = 1\ldots n$, see Table 1. In both scenarios, distances are normalized to $\max_{i=1\ldots n}\{r_i\}$.

Table 1 Vertices coordinates of n-gons with 5 and 7 sides

	i	1	2	3	4	5	6	7
Scenario								
#1	r_i	0.70	1.00	0.20	0.65	0.60	–	–
	φ_i (deg)	50	80	230	320	340	–	–
#2	r_i	0.85	1.00	0.70	0.55	0.65	0.60	0.50
	φ_i (deg)	15	30	70	140	190	210	330

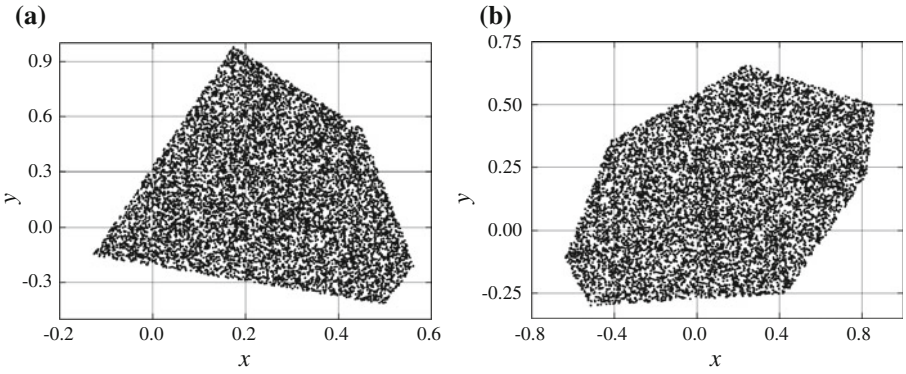

Fig. 3 Spatial distribution of points within the n-gons; Scenarios #1 (**a**) and #2 (**b**)

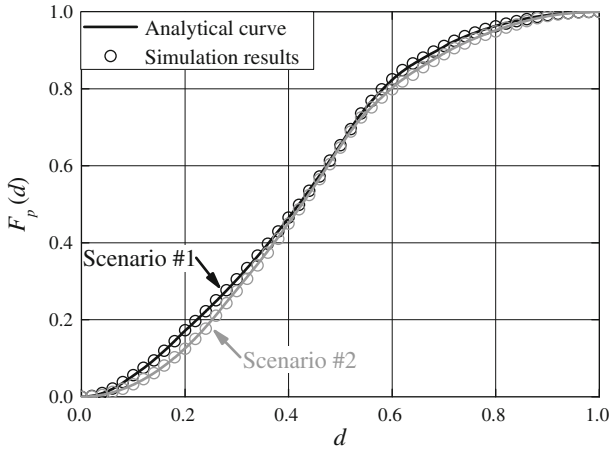

Fig. 4 Distance distribution: simulation results and analytical curves

In the simulations, a single node was randomly positioned for each snapshot within a unit circle centered at the coordinate origin. Next, the random points inside the n-gon were generated with the acceptance/rejection method (in order to do so, the sides of the n-gon were expressed in polar coordinates by using (13)) and the distance between each point and the origin was calculated. Figure 3a and b illustrates the spatial distribution of the generated points for the scenarios in Table 1 and 10^4 runs.

The analytical and simulated (for 10^6 independent runs) distance cdf and pdf curves are plotted in Figs. 4 and 5. The simulated values were averaged over a normalized distance size of 0.02. An excellent agreement between theory and simulation is observed. The pdf curves show peaks at the minimum distances at which the circle intersects the triangles' sides which are opposite to O; these peaks respond to the maxima of $\partial A_i/\partial d$, $i = 1 \ldots n$. Up to these distances, the intersection region between the circle and each of the triangles included in the n-gon is a circular sector and the derivatives $\partial A_i/\partial d$ increase linearly with d; see (19), (21) and (22).

In order to further validate and demonstrate the generalization of our approach, we compare it with the models discussed in Sect. 2 that refer to circular-, square- and hexagonal-shaped

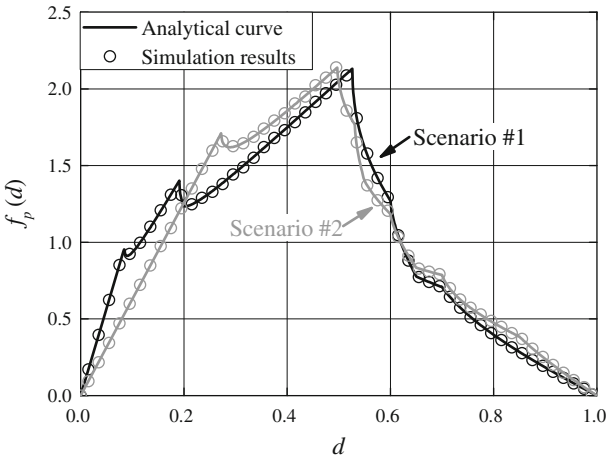

Fig. 5 Distance density: simulation results and analytical curves

Table 2 The proposed model as a generalization of models in the literature

Layout	Model	Fixed point position	Substitutions to obtain the statistics of other models	
			n	r_i, $\varphi_{i+1,i}$ (in deg), $i = 1 \ldots n$
Circular	Adelantado et al. [10]	Arbitrary	∞	$r_i = \sqrt{R^2 + D^2 + 2RD\cos\varphi_i}$, $\varphi_{i+1,i} = 360/n$
Square	Pirinen [19]	Center	4	$r_i = \text{const.}$, $\varphi_{i+1,i} = 90$
		Side midpoint	3	$r_{2,3} = \sqrt{5}r_1$, $\varphi_{2,1} \approx 63.43$, $\varphi_{3,2} \approx 53.13$
		Vertex	2	$r_2 = \sqrt{2}r_1$, $\varphi_{2,1} = 45$
Hexagonal	Zhuang et al. [5]	Vertex	4	$r_{2,4} = \sqrt{3}r_1$, $r_3 = 2r_1$, $\varphi_{i+1,i} = 30$
	Baltzis [13]	Center	6	$r_i = \text{const.}$, $\varphi_{i+1,i} = 60$

networks. It can be shown[2] that the aforementioned models and the corresponding distance cdfs and pdfs, deduce from the proposed model and (7), (20), respectively, with an appropriate choice of parameters as specified in Table 2.

In order to show the merits of our proposal, we provide in the following section a few representative examples in the study and analysis of wireless networks. In these examples, we assume a uniform node distribution; however, the outcomes of this analysis can be extended under certain conditions to networks with different node distribution such as the stationary Poisson point process [28].

5 Application Examples

Several issues in wireless networking are related to internode distance. Next, we use the obtained formulation to describe some distance-dependent network parameters and performance metrics and assess the impact of certain system characteristics on network performance. Applications in single-hop wireless networks with nearest- and farthest-neighbor routing [3,4,9,15,32–34] are also discussed. In particular, we present results for the distance

[2] The proof is straightforward and it is left to the reader.

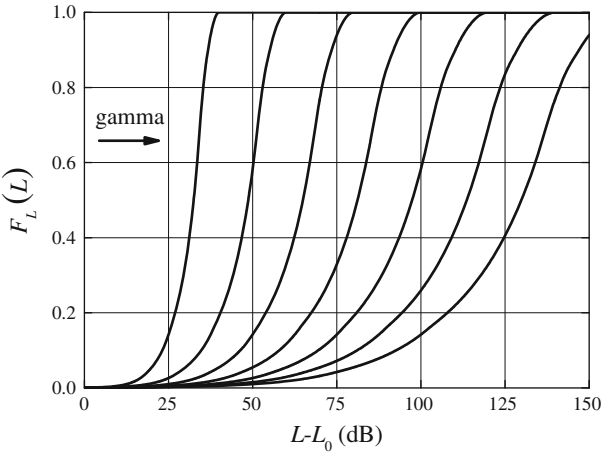

Fig. 6 Distance-dependent path loss cdf curves; γ varies from 2 to 8 with step one

dependent path loss, the sensitivity of WSNs, the minimum and maximum distance between nodes uniformly distributed within a network and the required energy for single-hop packet transmission in networks for different routing schemes. In the first three cases, the probabilistic distributions are expressed in closed form; however, analytical solutions for the expected distance and the consumed energy do not exist, even in simple scenarios such as the ones examined herein.

5.1 Distance Dependent Path Losses[3]

The distance-dependent path loss is usually described from an inverse power law [35–37]. In this case, the loss at a distance d greater than a reference distance d_0 that is chosen large enough to be in the far-field region of the transmitting antenna, is

$$L = L_0 \left(d/d_0\right)^{\gamma}, \quad d \geq d_0 \tag{24}$$

with L_0 the loss at d_0 and γ the path loss exponent. Thus, the distance-dependent path loss cdf and pdf are, respectively,

$$F_L(L) = P\left(d \leq d_0 \left(L/L_0\right)^{1/\gamma}\right) = F_p\left(d_0 \left(L/L_0\right)^{1/\gamma}\right), \quad L \geq L_0 \tag{25}$$

$$f_L(L) = \frac{\partial F_L(L)}{\partial L} = \frac{d_0 L^{-1+1/\gamma}}{\gamma L_0^{\gamma}} f_p\left(d_0 \left(L/L_0\right)^{1/\gamma}\right), \quad L \geq L_0 \tag{26}$$

with $P(X \leq x)$ the probability that a random variable X is lower than x.

As a sample application, we consider the pentagonal-shaped network with (normalized) vertices coordinates given in Table 1. We set $r_2 = 100\,\text{m}$ and assume that $d_0 = 1\,\text{m}$ [36]. Figure 6 shows the impact of path loss exponent on $F_L(L)$ for γ that ranges from 2 to 8 [37]. The x-axis represent the distance dependent path loss with reference to the loss at distance d_0. The cdf curves shift to the right with γ due to the increased signal absorption [12,13]; as a result, quantities that depend on the received signal strength such as the transmission range, the connectivity, the error probability, etc., show similar performance. This

[3] A generalization that includes small- and large-scale fading terms, though it is feasible, e.g. [13,27,35], leads to cumbersome mathematical expressions and it is omitted herein.

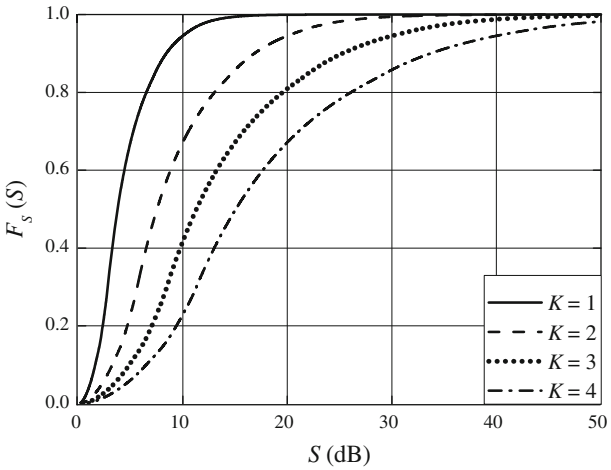

Fig. 7 Sensor sensitivity cdf curves for various K

shift depends on the maximum transmission range $d_{\max}$ (in this case, the r_2) and on d_0 and varies with L; from (24) and (25) comes that an increase in the path loss exponent equal to $\Delta\gamma$ shifts the cdf curve (in dB) from zero (for small values of $F_L(L)$) up to $10\Delta\gamma \log(d_{\max}/d_0)$ (when $F_L(L)$ approaches unity). Finally, we notice that the slope of the cdf curves decreases with γ.

5.2 WSNs' Sensitivity

In wireless sensor networks, the sensitivity of a sensor determines the establishment of a connection between two communicating nodes and diminishes with distance. In a simple sensitivity model with wide applicability [1,2], the sensitivity S of a sensor s at an arbitrary point Q at a distance d (s, Q) is given by the expression

$$S = \lambda\,[d\,(\mathrm{s},\mathrm{Q})]^{-K} \tag{27}$$

where λ, K are (positive) sensor-dependent parameters. Due to the stochastic nature of d (s, Q), S is a random variable with distribution and density functions:

$$F_S(S) = \mathrm{Prob}\left[d \geq (\lambda/S)^{1/K}\right] = 1 - F_p\left((\lambda/S)^{1/K}\right) \tag{28}$$

$$f_S(S) = \frac{\partial F_S(S)}{\partial S} = \frac{\lambda}{K S^{1+1/K}} f_p\left((\lambda/S)^{1/K}\right) \tag{29}$$

Figures 7 and 8 illustrate $F_S(S)$ and $f_S(S)$ for different K (typical values of this parameter range between 1 and 4 [1]) in a pentagonal-shaped network with vertices coordinates given in Table 1. Without loss of generality, we set $\lambda = 1$. We notice that both $F_S(S)$ and $f_S(S)$ depend strongly on K. Figure 7 further shows that the cdf curve shifts to the right with K which implies that an increase in K causes a significant degradation in the quality of sensing; moreover, the slope of the cdf curves decrease with K. From Fig. 8, we notice that S takes values in a limited range for $K = 1, 2$ but the pdf curves flatten noticeably with K, something that affects the transmission range, the network coverage, etc. The irregular shape of the pdf curves is due to the irregularities in the shape of the network coverage area. However, the curves become smoother when parameter K increases.

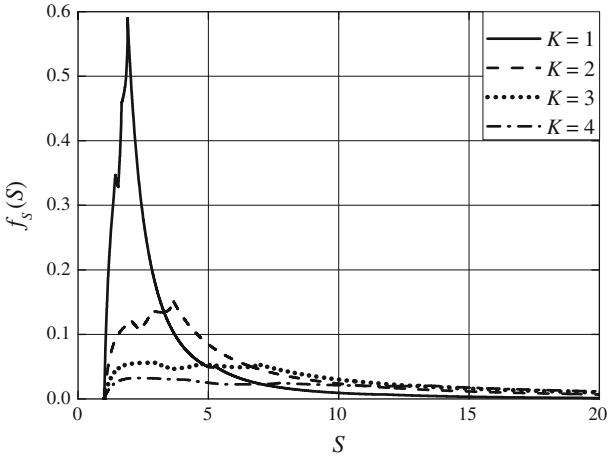

Fig. 8 Sensor sensitivity pdf curves for various K

5.3 Nearest/Farthest Neighbor Distributions in Sparse/Dense Networks

The knowledge of the nearest/farthest neighbor distribution is useful in protocol design. For example, in sparse networks with size greater than the communication range of the nodes, nearest-neighbor routing reduces energy consumption and increases throughput; on the other hand, in small dense networks, the choice of the farthest node as the packet forwarder minimizes the routing overhead, reduces the number of transmissions and improves connectivity [15,32,34].

Let us consider an n-gonal shaped wireless network with N randomly distributed nodes. The cdf, $F_\delta(\delta; N)$ and $F_\Delta(\Delta; N)$, and pdf, $f_\delta(\delta; N)$ and $f_\Delta(\Delta; N)$, functions of the minimum δ and maximum Δ, respectively, distance from the reference node to the rest $N-1$ ones can be written [15,28] as:

$$F_\delta(\delta; N) = 1 - \left[1 - F_p(\delta)\right]^{N-1} \tag{30}$$

$$f_\delta(\delta; N) = (N-1) f_p(\delta) \left[1 - F_p(\delta)\right]^{N-2} \tag{31}$$

$$F_\Delta(\Delta; N) = F_p^{N-1}(\Delta) \tag{32}$$

$$f_\Delta(\Delta; N) = (N-1) f_p(\Delta) F_p^{N-2}(\Delta) \tag{33}$$

As a representative example, we consider a pentagonal-shaped network (Scenario #1) and study the dependence of $f_\delta(\delta; N)$ and $f_\Delta(\Delta; N)$ on N. Without loss of generality, the distances are normalized to r_2, i.e., to $\max_{i=1\ldots n} \{r_i\}$; thus, different values of N imply networks with different size when the node density is fixed and vice versa. In Fig. 9 the nearest and farthest neighbor pdf for a set of N values is shown. Clearly, the spread of the curves decreases and the maxima of $f_\delta(\delta; N)$ ($f_\Delta(\Delta; N)$) shift to the left (right) with N, i.e., the hops become shorter in nearest-neighbor routing while in farthest-neighbor routing they practically reach the network boundary. Moreover, the curves become smoother at higher values of N and they have a more regular shape which approaches the shape of common statistical distributions [38]. In practice, this means that the irregularities of the shape of the network coverage area have a moderate effect on the shape of the nearest and the farthest neighbor pdf curves at large-scale and/or dense networks. A comparison between the two families of curves further

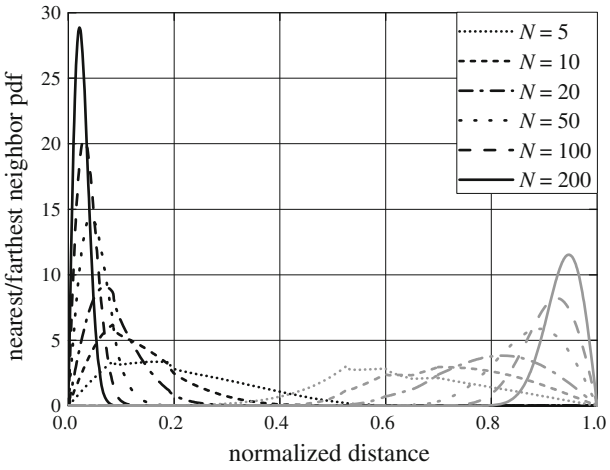

Fig. 9 Nearest (*black curves*) and farthest (*grey curves*) neighbor densities

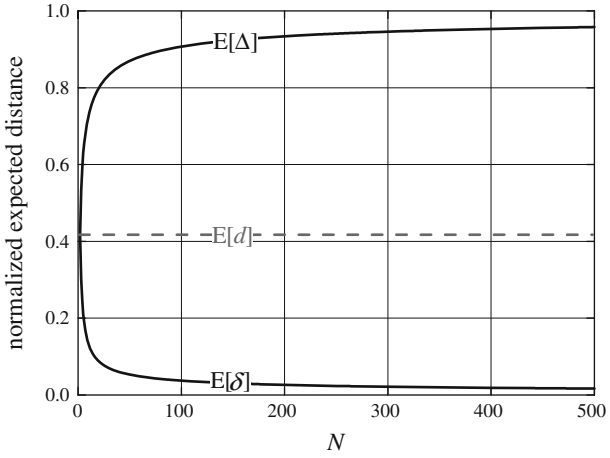

Fig. 10 Normalized expected distance as a function of N for single-hop transmission

exhibits the stronger dependence of $f_\delta(\delta; N)$ on N (the authors in [15] reached to similar conclusions for hexagonal-shaped networks).

The expectation of the distance to an arbitrary node, $\mathrm{E}[d]$, to the nearest neighbor, $\mathrm{E}[\delta]$, and to the farthest neighbor, $\mathrm{E}[\Delta]$, is obtained from the integration of the products $df_p(d)$, $\delta f_\delta(\delta; N)$ and $\Delta f_\Delta(\Delta; N)$, respectively, over the n-gon area. Let us consider the network in the previous example. Figure 10 plots the normalized expected distance for the three cases as a function of N. We notice that $\mathrm{E}[\delta]$ ($\mathrm{E}[\Delta]$) decreases (increases) with N, but as it increases, its impact on both quantities diminishes. The shape of the two curves for $N \gg 1$ implies, due to the uniform node distribution, that $\mathrm{E}[\delta]$ and $\mathrm{E}[\Delta]$ increase linearly with the area of the network size; at moderate values of N, the number of nodes affect more significantly the expected distance to the nearest neighbor, since the farthest node is already around the network boundary, see Fig. 9 (similar conclusions were drawn in [15] for regular hexagonal-shaped networks). Finally, it has to be noticed that the three curves coincide at $N = 2$, as it

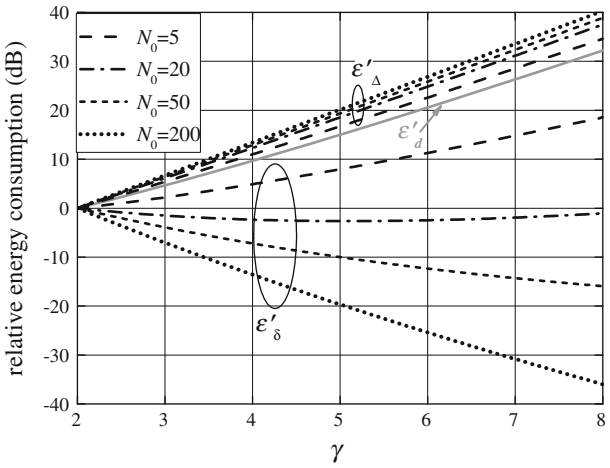

Fig. 11 Relative energy consumption versus γ for single-hop transmission ($\gamma_0 = 2$)

was expected from (31) and (33). Finally, the normalized expected distance to an arbitrary node, obviously, does not depend on N. Its value (0.417) is close to the arithmetic mean of $\mathrm{E}[\delta]$ and $\mathrm{E}[\Delta]$ for any N.

5.4 Energy Consumption

The required energy for packet transmission in a medium with attenuation that follows an inverse power law is proportional to the γth power of the link distance. In a simplistic approach, the average energy ε which is required for a single-hop transmission of a packet between two nodes is [4,5,7]

$$\varepsilon_D = k \int d^{\gamma} f_D(d)\, \mathrm{d}d \tag{34}$$

where k is an environment-dependent parameter proportional to the data rate while $f_D(d) \equiv f_\delta(d;N)$ ($f_\Delta(d;N)$) when the second node is the nearest (farthest) neighbor [4] and $f_D(d) \equiv f_d(d)$ if the second node is an arbitrary one [5,7]. Obviously, the integration in (34) is over the n-gon area.

As an application example, we consider the network of Scenario #1 and explore the impact of γ and N on the average required energy for the cases of single-hop transmission to an arbitrary node and to the nearest and farthest neighbor. In particular, we evaluate the dependence of the relative average energy consumption $\varepsilon'_D = \varepsilon_D - \varepsilon^0_D$ (in dB) on γ and N (subscript D stands for d, δ and Δ, and ε^0_D is the average consumed energy for given path loss exponent γ_0 or number of nodes N_0).

In Fig. 11, ε'_D is illustrated as a function of γ for the three cases. Clearly, the relative (average) energy consumption is a linear function of γ, due to the attenuation law, with slope that depends on the routing scheme and the number of nodes. In nearest-neighbor routing, power consumption decreases with γ because signal transmission employs nodes that are close to each other (similar results were derived in [32,33]). As it was expected, power consumption increases with γ in the case without routing and in the farthest-neighbor routing scheme (in general, at single large hops, attenuation is proportional to the γth power of the transmission distance [8]). Notice also that ε'_δ (ε'_Δ) decrease (increase) with N. This

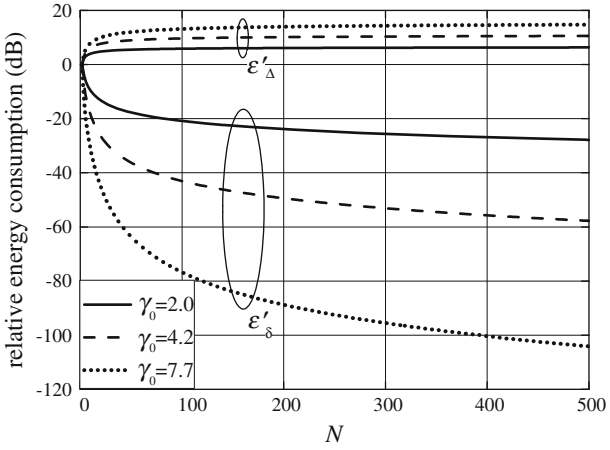

Fig. 12 Relative energy consumption versus N for single-hop transmission ($N_0 = 2$)

behavior is easily explained from the dependence of $f_\delta(\delta; N)$ and $f_\Delta(\Delta; N)$ on N, see Fig. 9 (recall that the maxima of $f_\delta(\delta; N)$ ($f_\Delta(\Delta; N)$) shift to the left (right) with N. Moreover, the impact of N is more intense on ε'_δ.

Similar conclusions are obtained from Fig. 12 that shows ε'_Δ and ε'_δ versus N. The cases $\gamma_0 = 2, 4.2$ and 7.7 (typical values for free-space, urban and dual carriage highway propagation, respectively [37]) are presented. Generally, in single-hop transmission, the impact of γ and N on energy consumption is more intense in nearest-neighbor routing. In fact, in farthest-neighbor routing, the number of nodes does not affect noticeably power consumption because the farthest node is close to the network boundaries; however, even in nearest-neighbor routing, the impact of N on energy consumption diminishes with increasing N.

6 Conclusions

In this paper, we presented the mathematical framework for the analytical description of the Euclidean distance distribution in an arbitrary n-gon. The proposed method can also be regarded as a generalization of simpler models in the literature. Simulation results validated the proposal. In order to show the applicability of the model, we further discussed representative applications in wireless networking. Interesting conclusions for the impact of channel attenuation, number of nodes and routing scheme on system performance were obtained. The analytical description of distance statistics allows the estimation of distance-dependent metrics, offers the capability of determining optimum network parameters and assists in network planning and routing. The derived formulation simplifies the analysis of wireless networks and reduces the computational requirements of system-level simulations.

References

1. Megerian, S., Koushanfar, F., Qu, G., Veltri, G., & Potkonjak, M. (2002). Exposure in wireless sensor networks: Theory and practical solutions. *Wireless Networks, 8*(5), 443–454.
2. Ghosh, A., & Das, S. K. (2008). Coverage and connectivity issues in wireless sensor networks: A survey. *Pervasive and Mobile Computing, 4*(3), 303–334.

3. Haenggi, M., Andrews, J. G., Baccelli, F., Dousse, O., & Franceschetti, M. (2009). Stochastic geometry and random graphs for the analysis and design of wireless networks. *IEEE Journal on Selected Areas in Communications, 27*(7), 1029–1046.
4. Srinivasa, S., & Haenggi, M. (2010). Distance distributions in finite uniformly random networks: Theory and applications. *IEEE Transactions on Vehicular Technology, 59*(2), 940–949.
5. Zhuang, Y., Luo, Y., Cai, L., & Pan, J. (2011). A geometric probability model for capacity analysis and interference estimation in wireless mobile cellular systems. In *54th IEEE global telecommunications conference (GLOBECOM'11)*, Houston, USA. doi:10.1109/GLOCOM.2011.6134503.
6. Sinanović, S., Serafimovski, N., Haas, H., & Auer, G. (2008). Maximizing the system spectral efficiency in a decentralised 2-link wireless network. *EURASIP Journal on Wireless Communications and Networking*. doi:10.1155/2008/867959.
7. Heinzelman, W. B., Chandrakasan, A. P., & Balakrishnan, H. (2002). An application-specific protocol architecture for wireless microsensor networks. *IEEE Transactions on Wireless Communications, 1*(4), 660–670.
8. Zhuang, Y., Pan, J., & Cai, L. (2010). Minimizing energy consumption with probabilistic distance models in wireless sensor networks. In *29th IEEE international conference on computer communications (INFOCOM'10)*, San Diego, USA. doi:10.1109/INFCOM.2010.5462073.
9. Gopakumar, A., & Jacob, L. (2011). Power-aware range-free wireless sensor network localization using neighbor distance distribution. *Wireless Communications and Mobile Computing*. doi:10.1002/wcm.1113.
10. Adelantado, F., Pérez-Romero, J., & Sallent, O. (2007). Nonuniform traffic distribution model in reverse link of multirate/multiservice WCDMA-based systems. *IEEE Transactions on Vehicular Technology, 56*(5), 2902–2914.
11. Chang, S. Y., & Wu, H.-C. (2011). Statistical analysis for large-scale hierarchical networks using network coding. *IEEE Transactions on Vehicular Technology, 60*(5), 2152–2163.
12. Baltzis, K. B. (2011). A geometric method for computing the nodal distance distribution in mobile networks. *Progress in Electromagnetics Research, 114*, 159–175.
13. Baltzis, K. B. (2011). Analytical and closed-form expressions for the distribution of path loss in hexagonal cellular networks. *Wireless Personal Communications, 60*(4), 599–610.
14. Ali, A., Latiff, L. A., & Fisal, N. (2010). Simulation-based real-time routing protocol with load distribution in wireless sensor networks. *Wireless Communications and Mobile Computing, 10*(7), 1002–1016.
15. Zhuang, Y., & Pan, J. (2012). A geometrical probability approach to location-critical network performance metrics. In 31st IEEE international conference on computer communications (INFOCOM'12), Orlando, USA. http://grp.pan.uvic.ca/~yyzhuang/hexagon.pdf. Accessed 7 May 2012.
16. Xiao, L., Greenstein, L. J., Mandayam, N. B., & Periyalwar, S. (2008). Distributed measurements for estimating and updating cellular system performance. *IEEE Transactions on Communications, 56*(6), 991–998.
17. Choi, S.-O., & You, K.-H. (2008). Channel adaptive power control in the uplink of CDMA systems. *Wireless Personal Communications, 47*(3), 441–448.
18. Mullen, J. P. (2003). Robust approximations to the distribution of link distances in a wireless network occupying a rectangular region. *Mobile Computing and Communications Review, 7*(2), 80–91.
19. Pirinen, P. (2006). Outage analysis of ultra-wideband system in lognormal multipath fading and square-shaped cellular configurations. *EURASIP Journal on Wireless Communications and Networking*. doi:10.1155/WCN/2006/19460.
20. Bai, X., Kumar, S., Xuan, D., Yun, Z., & Lai, T. H. (2006). Deploying wireless sensors to achieve both coverage and connectivity. In *7th ACM International Symposium on Mobile Ad Hoc Networking and Computing (MobiHoc'06)*, Florence, Italy, pp. 131–142.
21. Zhuang, Y., & Pan, J. (2011). *Random distances associated with rhombuses*. http://arxiv.org/pdf/1106.2200.pdf. Accessed 7 May 2012.
22. Melodia, T., Pompili, D., & Akyildiz, I. F. (2010). Handling mobility in wireless sensor and actor networks. *IEEE Transactions on Mobile Computing, 9*(2), 160–173.
23. Noori, M., & Ardakani, M. (2011). Lifetime analysis of random event-driven clustered wireless sensor networks. *IEEE Transactions on Mobile Computing, 10*(10), 1448–1458.
24. Li, W., Martins, P., & Shen, L. (2012). Determination method of optimal number of clusters for clustered wireless sensor networks. *Wireless Communications and Mobile Computing, 12*(2), 158–168.
25. Ganti, R. K., & Haenggi, M. (2009). Interference and outage in clustered wireless ad hoc networks. *IEEE Transactions on Information Theory, 55*(9), 4067–4086.
26. Stamatiou, K., Proakis, J. G., & Zeidler, J. R. (2010). Channel diversity in random wireless networks. *IEEE Transactions on Wireless Communications, 9*(7), 2280–2289.

27. Alouini, M.-S., & Goldsmith, A. J. (1999). Area spectral efficiency of cellular mobile radio systems. *IEEE Transactions on Vehicular Technology, 48*(4), 1047–1066.
28. Moltchanov, D. (2012). Distance distributions in random networks. *Ad Hoc Networks, 10*(6), 1146–1166.
29. Voronoi diagrams. http://www-sop.inria.fr/prisme/fiches/Voronoi/index.html.en. Accessed 7 May 2012.
30. MathWorld–A Wolfram web resource. Circle-line intersection. http://mathworld.wolfram.com/Circle-LineIntersection.html. Accessed 7 May 2012.
31. Vizireanu, D. N., & Halunga, S. V. (2011). Single sine wave parameters estimation method based on four equally spaced samples. *International Journal of Electronics, 98*(7), 941–948.
32. Haenggi, M., & Puccinelli, D. (2005). Routing in ad hoc networks: A case for long hops. *IEEE Communications Magazine, 43*(10), 93–101.
33. Bush, S. F. (2005). Low-energy sensor-network time synchronization as an emergent property. In *14th International conference on computer communications and networks (ICCN'05)*, San Diego, USA, pp. 93–98.
34. Luo, D., Zuo, D., & Yang, X. An energy-saving routing protocol for wireless sensor networks. In *4th International conference on wireless communications, networking and mobile computing (WiCOM'08)*, Dalian, China. doi:10.1109/WiCOM.2008.964.
35. Baltzis, K. B. (2010). Closed from description of microwave signal attenuation in cellular systems. *Radio Engineering, 19*(1), 11–16.
36. Rappaport, T. S. (2002). *Wireless communications: Principles and practice* (2nd ed.). Upper Saddle River: Prentice Hall.
37. Agbinya, J. I. (2007). Design considerations of MoHotS and wireless chain networks. *Wireless Personal Communications, 40*(1), 91–106.
38. Shankar, P. M. (2011). Statistical models for fading and shadowed fading channels in wireless systems: A pedagogical perspective. *Wireless Personal Communications, 60*(2), 191–213.

Author Biography

Konstantinos B. Baltzis was born in Thessaloniki, Greece in 1973. He holds a B.Sc. degree in Physics, a M.Sc. degree in Communications and Electronics, and a Ph.D. degree in Communications Engineering. He is a research associate in the Radio Communications Laboratory of the Aristotle University of Thessaloniki (AUTh) and a teaching staff member at the Program of Postgraduate Studies in Electronic Physics of AUTh. Dr. Baltzis is an IEEE Senior Member and a member of the editorial board of the Radio engineering journal and the Journal of Wireless Networking and Communications. He has authored or co-authored more than fifty articles in international peer-reviewed journals and conferences and contributed two book chapters. His current research interests include wireless communications systems, ad-hoc networking, radio propagation, antennas design, and evolutionary optimization methods.